Progress on Design and R&D of CN Solid Breeder TBM *FTP/3-5Ra*

K.M. Feng, G.S. Zhang, T.Y. Luo, Z. Zhao, Y.J. Chen, X.F. Ye, G. Hu, P.H. Wang.

T. Yuan, Y.J. Feng, B. Xiang, L. Zhang, Q.J. Wang, Q.X. Cao, F.Wang, Z.X. Li,

and Chinese HCSB TBM team

Southwestern Institute of Physics, Chengdu 610041, P.R. China
Email: *fengkm@swip.ac.cn; Fax:+86-28-82850956*

ABSTRACT

Current progress on the design and R&D of Chinese helium-cooled solid breeder test blanket module，CN HCSB TBM is presented. The updated design on structural, neutronics, thermal-hydraulics and safety analysis has been completed. In order to accommodate the HCSB TBM ancillary system, the design and necessary R&Ds corresponding sub-systems have being developed. Current status on the development of function materials, structure material and the helium test loop are also presented. The Chinese low-activation ferritic/martensitic steels CLF-1, which is the structural material for the of HCSB TBM is being manufactured by industry. The neutron multiplier Be and tritium breeder Li_4SiO_4 pebbles are being prepared in laboratory scale.

1. Introduction

ITER will be used to test tritium breeding module concepts, which will lead to the design of DEMO fusion reactor design demonstrating tritium self-sufficiency and the extraction of high grade heat for electricity production. The helium-cooled/solid tritium breeder (HCSB) with the pebble bed concept was selected as Chinese test blanket module (TBM) design. Dimensions of HCSB TBM occupying half of the ITER test port is shown in Fig.1. Previous configuration of the HCSB TBM with the 3×6 modularized sub-module (SM) arrangement has been replaced by the 2×6 modularized SM arrangement [1]. The new configuration will better satisfy the ITER TBM design requirements [2]. Corresponding design optimization on structural, neutronics, and detailed performance analyses has been performed. Furthermore, in order to reduce the impacts of the RAFM steel material impact on the magnetic field ripple, the last design has been modified to minimize the mass of RAFM steel.

Updated structure design based on originally design that is shown in Figs.1-2 has been performed. Progress on module configuration, analysis on structure, neutronics, thermal hydraulic, thermal mechanical, EM assessment on induced field ripple are presented. Necessary R&Ds on the low-activated CLF-1 steel, neutron multiplier Be pebbles, and the tritium breeding materials Li_4SiO_4 pebbles are moving towards industrial production level.

2. Modification Design

Main design modification of HCSB TBM is focuse on the structure and configuration of breeding zone of the sub-module. In the former design, the backside of the blanket module is

the back-plate forming the flow plenum and distributors. The stiffening grid plate is welded into the box; and each grid plate is cooled by helium flowing with internal channels that are fed from the back. Breeding sub-modules (shown in Fig.2) are separated by the grid plates. Each sub-module has its own independent cooling and tritium purge gas circuits. Tritium breeder and neutron multiplier are separated by the cooling channel of the sub-module.

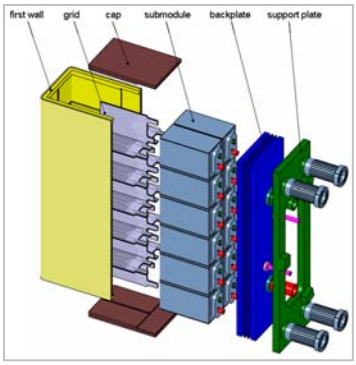

Fig.1. Schematic view of the HCSB TBM

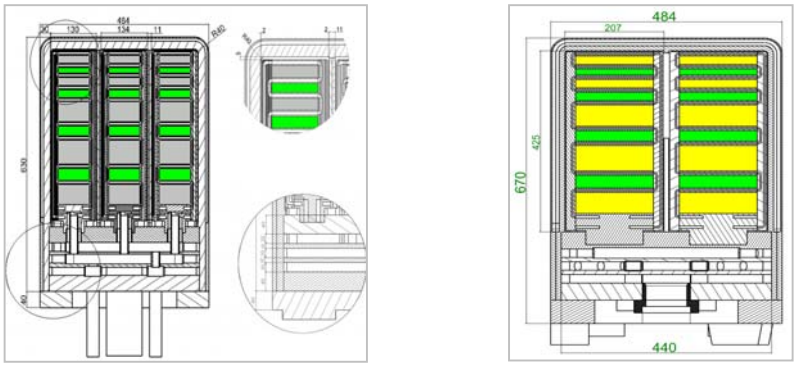

(1) (2)

Fig.2. 2-D model of the HCSB TBM blanket module [1]

(1) 3×6 arrangement of sub-modules (2) Modified 2×6 arrangement of sub-module

The structure design of the sub-module has been modified based on the neutonics results from a 3-D MCNP global model. The modified configuration of the HCSB TBM is shown in Fig.3a. Main modifications of new modular design include: (1) The TBM is composed of two materials; RAFM steel is used for the FW, caps, grid and sub-modules section, and 316 stainless steel is used for the back-plate and support-plate. (2) The total radial length of the TBM is retained at 670mm, but the radial dimension of the U-shape FW and breeder sub-modules were decreased to 350 mm and 320mm, respectively. Subsequently, the total mass of the RAFM steel in TBM is reduced to 720 kg. The explored view of the TBM module is shown in Fig.3b. (3) The width of the CP is decreased by 5mm while keeping the area of the cross-section of the helium gas channel. (4) Arrangement of pebble beds in sub-module is changed from the former transverse direction to the current vertical direction, which has the advantages of simplifying the helium cooling loop, improving the neutronics performance. The corresponding RAFM steel of the the sub-module is reduced. Schematic of the sub-module is shown in Fig.3c. Main parameters of the modified HCSB TBM design are listed in Table 1.

Table 1 Main parameters of HCSB TBM

Neutron wall loading (MW/m^2)	0.78
Max. surface heat flux (MWm^2)	0.50
Tritium production rate (g/day)	0.0707
Max. power density, (MW/m^3)	10.64
Tritium breeder	Lithium orthosilicate, Li_4SiO_4
Form	Diameter (D)=1.0mm, pebble bed
^{6}Li Enrichment, %	80
Peak temperature (°C)	703
Neutron multiplier	Beryllium
Form	Binary, Diameter (D)=0.5mm-1.0mm, pebble bed
Peak temperature (°C)	516
Coolant	Helium (He)
Pressure (MPa)	8
Tin / Tout (°C)	300 / 500
Pressure drop (Δ p)	0.12
Structural material	LAFM(CLF-1)
Max. temperature (°C)	516

Presently, the modified HCSB TBM has the FW coolant flow routed in the poloidal direction, as shown in Fig.3a and Fig.3b. Every 3 poloidal coolant channels are to form a cooling loop, with a total of 9 loops cooling the FW. Moreover, the modified sub-module has three breeder and multiplier zones. The cross-section of the sub-module is shown in Fig.3c.

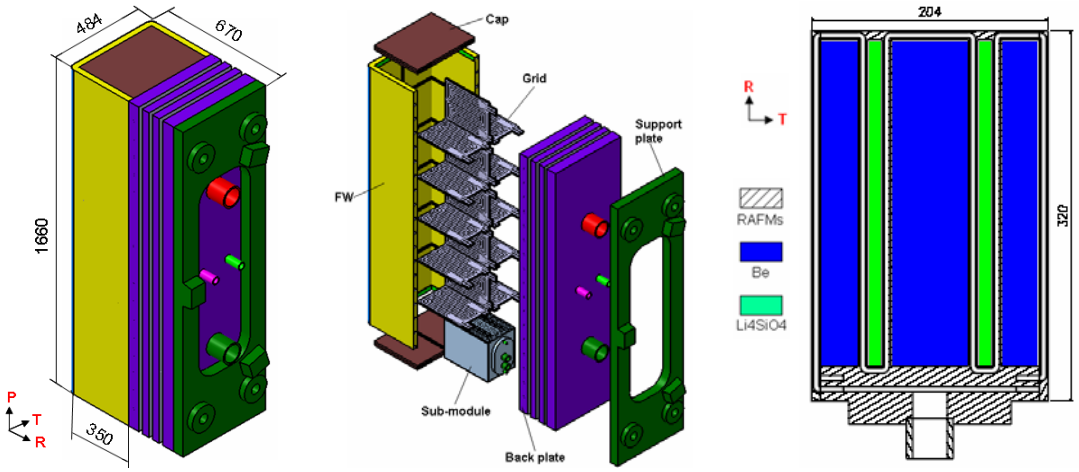

a) Isometric view of TBM b) Explosive view of TBM c) Cross-section view of sub-module

Fig.3 Modified design of HCSB TBM

At the TBM's back-plate there are two helium systems, the Helium Coolant Manifold System (HCMS) and the Purge Gas Manifolds System (PGMS). The structure of the back-plate was shown in Fig.4. The larger pipes are helium inlet, outlet and bypass. Their diameters are 85.5 mm inside and 101.6mm outside, the smaller pipe diameters are 30mm inside and 35mm outside are for purge gas inlet and outlet flows. The coolant inlet pipe is attached to outside plate, and the remaining pipes are attached to closure plates. Ribs are used

to connect the outside plate, middle plate and the inside plate in back-plate. These also plates form the coolant manifolds. Between the outside plate and inside plate, there are 2 middle plates. Conducting pipes are set between two middle plates. The temperature distribution of back-plate is shown in Fig.5.

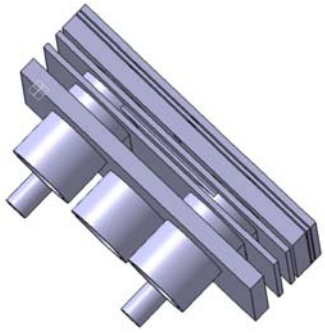

Fig.4 Structure view of back-plate of HCSB TBM

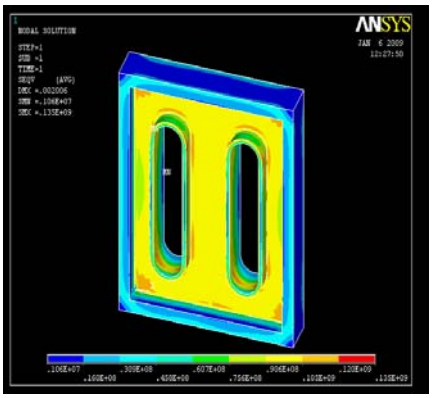

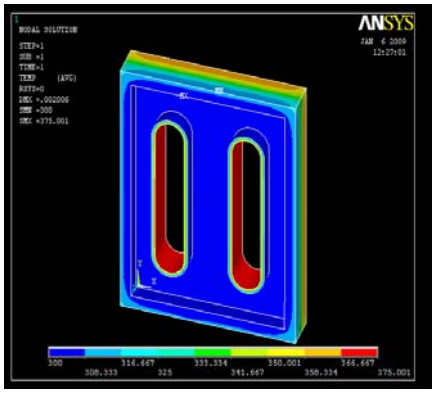

(1) Stress distribution (2) Temperature distribution

Fig.5 Stress and temperature distribution of back-plate

3. Performance analyses

3.1 Thermal mechanical

Neutronics results based on 3-D MCNP model were generated for the optimized design are shown in Table 2. It was shown that the neutronics performance of modified module design is obviously improved comparison with former design. These results were used as basic input parameters for the of HCSB TBM analysis. Fig.5 shows results of the thermal and mechanical analysis for the middle plate and back-plate of the TBM sub-module. Temperature distribution between ranges of 300-500 ºC is shown. The calculated maximum stress is 135MPa as shown in the right, which is lower than the 3Sm allowable stress requirement. Fluid flow analysis was also performed. With the total coolant mass flow rate of 1.3kg/s, the minimum flow into the first channel is 0.0705kg/s while the maximum is 0.0740kg/s. Fluid flow balance will be modeled in the future. Thermal hydraulic parameters of the HCSB TBM are listed in Table 3.

Table 2 Neutronics paramers of HCSB TBM

Parameters	Original design	Modified design
Max neutron flux, （n/s.cm^2）	2.36×10^{14}	2.36×10^{14}
Neutron wall loading, （MW/m^2）	0.78	0.78
Tritium production rate , （g/d）	0.0560	0.0797
Total nuclear heat deposition, （MW）	0.587	0.681
Max. power density, （MW/m^3）	6.26	10.64

Table 3 Thermal hydraulic parameters of CH HCSB TBM

Neutron surface loading [MW/m^2]		0.78	
Surface heat flux [MW/m^2]		0.50	
Total power [MW]		0.99	
Helium pressure [MPa]		8	
Helium inlet/outlet temperature [℃]		Velocity of helium [m/s]	
First wall	300/375	First wall	63
Grid/caps	375/386	Grid$_h$ / Grid$_v$ / caps	37/38/39
Sub-module	386/496	Sub-module	17
Mass flow rate of helium [kg/s]		Pressure drop of helium [MPa]	
First wall	1.33	First wall	0.21
Grid/caps	0.36/0.36	Grid$_h$ / Grid$_v$ / caps	0.03/0.03/0.04
Sub-modules	0.73	Sub-module	0.03
By-pass	0.6	Total (including external circuit)	0.35 (~0.1)
Equivalent diameter of channel [mm]		Heat transfer coefficient [W/(m^2.K)]	
First wall	13.7	First wall	4329
Grid$_h$ / Grid$_v$ / caps	6.9/7.5/20	Grid$_h$ / Grid$_v$ / caps	3324/3331/2640
Sub-modules	6	Sub-modules	1845

During the D-T phase of ITER, the average heat flux on the FW of TBM during normal plasma operation is 0.27 MW/m^2. The maximum heat load is 0.5MW/m^2 taking into account MARF and other physics phenomena; it would last for about 10 seconds [3]. Assuming the maximum heat load to occur in the middle of the burn time as shown in Fig.6, transient thermal analysis results of FW are shown in Fig.7. Since the duration of the maximum heat flux is very short during the plasma burn period the maximum temperature of the FW reaches 513℃ when the coolant temperature is at 362 ℃.

During plasma disruption, with the peak energy flux deposition at 0.55MJ/m^2 in 1 ms, with the corresponding heat flux of about 550MW/m^2 and follow by the subsequent energy flux of 0.72MJ/m^2 during the next 40 ms with corresponding heat flux of about 18MW/m^2 [4]. Fig.8 shows the temperature response of the beryllium layer and the RAFM steel substrate. Both have an acute rise in 1.4 ms, after which, the temperature is slightly increased both in Be and RAFM steel due to the mean value of 18MW/m^2 for the analysis for the duration of 40

ms.

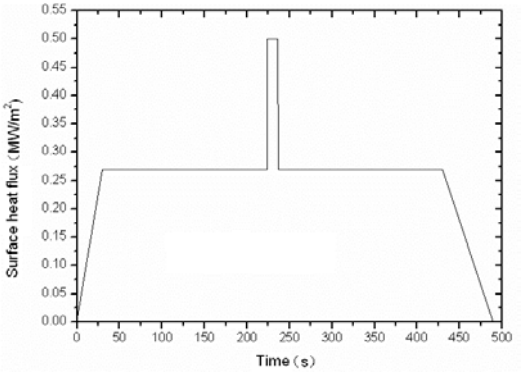

Fig 6 Surface heat load condition of FW

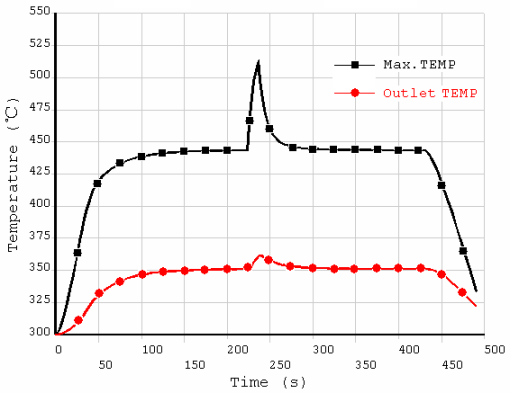

Fig.7 Transient thermal analysis for the FW

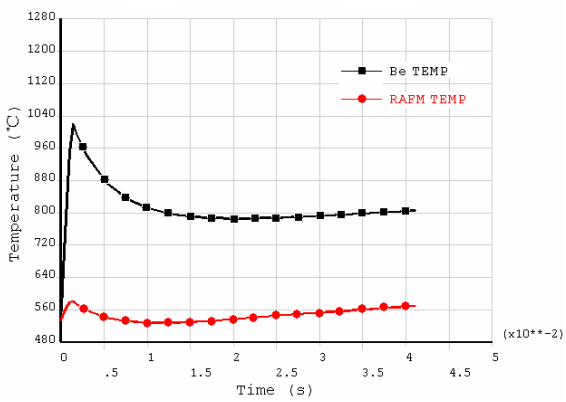

Fig.8 FWs temperature in case of plasma disruption

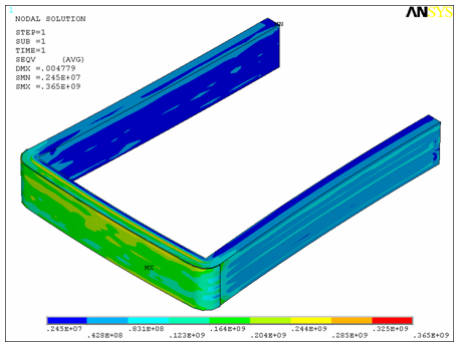

Fig.9 Stress of FW （Be used as the armor）

The preliminary mechanical analysis results of FW were shown in Fig.9. The maximum stress of RAFM steel is 365 MPa which can meet the 3Sm allowable stress requirement [4], but that of beryllium layer is 281MPa which is outside the allowable stress. Compared with that of Be, the yield strength of W is high [5], but there is a big difference of thermal expansion coefficient between W (4.16×10^{-6}/K) and RAFM steel (11.9×10^{-6}/K) which will result in a high stress at their interface, so it is suggested the use of the W/Cu alloy as the interface material (the thermal expansion coefficient of Cu is about 18.9×10^{-6}/K [5]), in virtue of the thermal expansion coefficient of W/Cu alloy can be controlled by adjusting the material composition. As shown from Fig.9, it can be seen that the maximum stress of both

RAFM steel and W/Cu alloy have an obvious decrease with increase of the thermal expansion coefficient of W/Cu alloy to about 9×10^{-6}/K.

3.2 EM stress analyses

Based on the ITER classifications of load specification, the assumptions for plasma disruption are 40 ms for current decay time and 18 ms for exponential decay [6-7]. During plasma disruption mechanical forces and stresses can be produced due to the interaction between the eddy currents induced in TBM and the magnetic fields.

Detailed analytical results based on two disruption models are shown in Fig.10-11. Due to poloidal magnetic field the rapid variation of the maximum eddy current can be induced and move along the radial-toroidal direction. By the calculation on magnetic-structural coupling, results show that the maximum Tresca stress occurs at the manifold in the TBM because of its box configuration and with constraintsby the supporting plate. The maximum Tresca stress appears during plasma current exponential decay with a value of 33.2MPa which is within allowable value (the maximum allowable stress is 365MPa for the reference CLF-1 steel at 300K) [8].

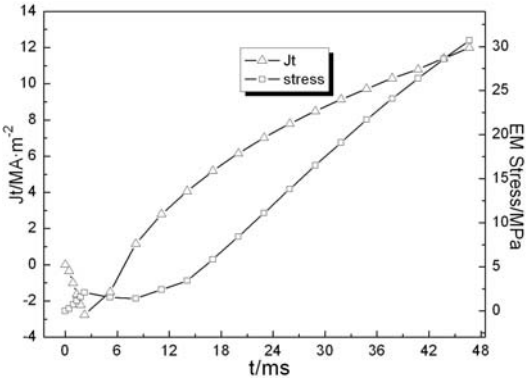

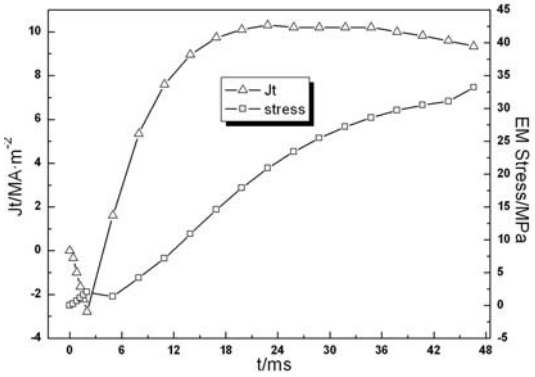

Fig.10. Eddy current and mechanical stress change with linear disruption Fig.11. Eddy current and mechanical stress change with exponential disruption

3.3 TBM-inducing TF ripple analyses

The magnetization of ferromagnetic material in the TBM would produce a non-axisymmetrical magnetic field which can increase the TF ripple. Calculations showed that the B_{TF} was 5.31T at 6.2m of major radius. Comparing the TF ripple without TBM exceeded 1% at the plasma edge where TBM faces, requiring the intervention of some correcting elements such as the introduction of the ferromagnetic inserts (FIs) and/or the decrease of ferromagnetic materials in TBM. To study the ferromagnetic effects on TF ripple, two models were used for the CN HCSB-TBMs with different amount of ferromagnetic material, and with the use of FIs of different magnetic saturation materials [9].

The analyses based on Figs.12-13 showed that The TF ripple increased significantly to ~5% because of the intervention of TBMs, which were assumed to occupy the whole TBMs with ferromagnetic steel and its weight was ~4.8 tons. However, the ripple can be lowered to ~1.9% when the weight of TBM reduced to ~2.6 tons. It has been found that it was remarkable to reduce ripple by decreasing the ferromagnetic steel in TBM. At the same time the ripple produced by TBM can be reduce to ~0.4% through the introduction of FIs with magnetic

saturation at 1.47T. It has been concluded that it was feasible reduce the TBM-inducing TF ripple by taking fully account of the combination of changing the amount of the ferromagnetic material used and the addition of ferromagnetic material inserts.

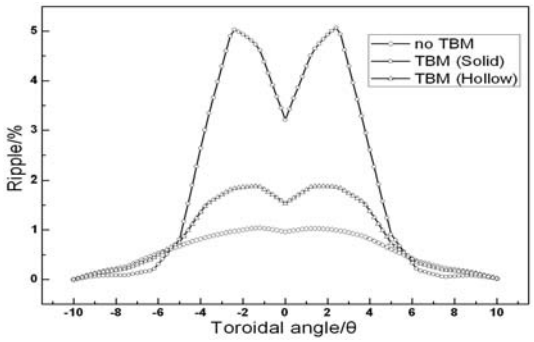

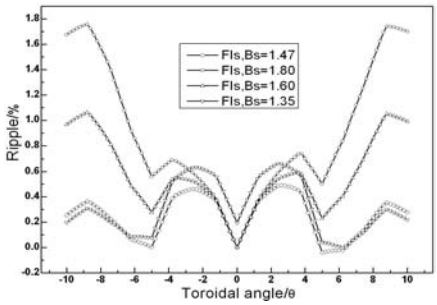

Fig.12. ripple distribution at R=8.2m, Z=0.38m without FIs (hollow TBM)

Fig.13. Ripple distribution at R=8.2m, Z=0.38m with hollow TBM

3.4. Probabilistic Safety Analysis

A preliminary probabilistic safety analysis of the system has been carried out to analyze and check the safety properties of system. The analysis mainly focuses on qualitative study and also includes a rough quantitative estimation.

Uncontrolled energy could cause accidents or aggravate their consequences. The energy sources in the system include 0.681MW nuclear thermal power during normal operation, 1.02 MJ energy deposited onto the TBM during a plasma disruption, as well as afterheat from the decay heat of activated productions when fusion power is terminated during shutdown. The initial afterheat is very small and keeps decreasing over time. The hazard sources which could affect operators, public or environmental safety if exposed was determined. The most dangerous radioactive source is tritium due to the high mobilization potentiality of the tritium gas and tritiated water. The tritium inventory in system includes 5.2 mg in the breeder, 0.1 mg in the Be multiplier, 2 mg in helium cooling system (HCS) and 30mg in tritium extraction system (TES). Measures adopted in the system to prevent, control and mitigate accidents were identified, including hazards confinement, heat removal, pressure control, isolation,detection of abnormal events, fusion power termination and detritiation.

Table 4 Consequence severity and probability

PIE	Description	Probability ($year^{-1}$)	Consequences severity	Risk
FB1	Completely lost of coolant flow	2e-1	0.14	0.003
FB2	Partly lost of coolant flow	5e-2	7.3e-4	3.7e-5
HB1	Lost of HCS heat sink	1e-1	7.3e-4	7.3e-5
LBB1	LOCA in TBM box, rupture of cooling channel	1e-3	9.0	0.009
LBB2	LOCA in TBM box, leak of cooling channel	1e-2	0.73	0.007
LBV1	LOCA in VV, rupture of TBM first wall	1e-3	17.9	0.018
LBV2	LOCA in VV, leak of TBM first wall	1e-2	7.3	0.073
LBO1	LOCA out VV, large rupture of HCS in TWCS	1e-2	19.4	0.19

LBO2	LOCA out VV, small rupture of HCS in TWCS	1e-1	3	0.3
LBO3	LOCA out VV, rupture of tubes in heat exchanger	1e-2	9.1	0.09
LBP1	LOCA out VV, large rupture of HCS in port cell	1e-3	21.4	0.021
LBP2	LOCA out VV, small rupture of HCS in port cell	1e-2	3	0.03
LEL1	Small rupture of TES process line inside T-building glove box	1e-3	5.1	0.005
LEL2	Small rupture of TES process line inside Port Cell	1e-3	6.1	0.006

Postulated Initial Events (PIE) are obtained from FMEA method similar to previous studies [10] and listed in the Table 4. Probability data was roughly estimated by comparison with events in previous work [11, 12]. Various potential consequences were analyzed, up to now only non-dimensional severity numbers were assigned by the comparison of the severities of different events. Accident sequences and safety system responses of every PIE were logically modeled using event trees. Fig 14 shows the event tree of PIE LBB1 (Large LOCA in TBM box) in TES, which is one of them. Probability of every tree branches are calculated from event trees, and risks are obtained then. The analysis shows that safety measures like timely terminating of the fusion power, appropriate isolation systems and the application of reliable pressure suppression systems can effectively reduce accident risk [13]. Future design modification will be based on these results in order to enhance the system safety.

.

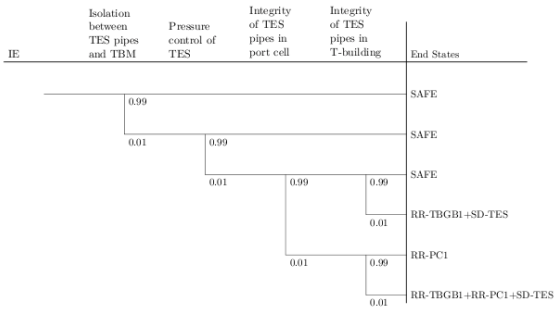

Fig.14 The event tree of PIE LBB1 in TES

4. Progress on R&D

Some of test facilities including TBM Electromagnetism test facility and Helium Loop operating at high pressure and temperature as part of the test blanket system prior to TBMs installation in ITER have being built. Relevant R&D on the key issues of the tritium system, RAFM structure material CFL-1, the function materials including the solid breeder and neutron multiplier fabrication technology as well as the tritium permeation barriers, etc. have being developed.

4.1 Structure material

The reduced activation RAFM steel was selected to serve as the fusion structural material. CLF-1 is the Chinese product of this RAFM steel for the CH HCSB TBM. The

objective of CLF-1 structural material R&D is to provide materials for the fabrication of the CH HCSB TBM and to provide the basic material properties database and corresponding technical information required for blanket fabrication, e.g. strength, ductility, ductile-to-brittle transition temperature (DBTT), heat treatment conditions joining conditions and thermal and physical properties.

A 350kg of CLF-1 steel was recently produced by vacuum induction melting and electroslag remelting method. The ingot was hot forged and hot rolled into different plates and rods. The chemical composition of the CLF-1 steel is Fe-8.5Cr-1.5W-0.25V-0.5Mn-0.1Ta-0.1C (wt.%) and in addition 0.025wt.%N is added to keep the phase stable during the long time thermal ageing. The radiological undesirable tramp elements such as Nb and Mo were reduced down to 0.001% and 0.005%, respectively. Heat treatment conditions for the plates including normalization (980ºC/45min, air-cooled) and tempering (740ºC/90min, air-cooled) were selected to get the best trade-off between strength and ductility.

Some mechanical properties such as tensile and impact properties have been tested. Some physical properties have also been determined. Table 5 presents the thermal properties of CLF-1. The preliminary TIG welding experiments have been done and the welds show properties that make the welding techniques applicable for TBM manufacturing. The helium retention and description behavior was investigated using an ECR ion irradiation apparatus [14]. The metallurgical properties of CLF-1 were been investigated after thermal ageing treatments performed at 550ºC and 600ºC up to 5000h, and the steel did not exhibit significant microstructural changes.

Table 5 Thermal properties of CLF-1

Test temperature (℃)	Thermal Diffusivity ($10^{-6}m^2/s$)	Specific heat (J/kg·℃)	Thermal Conductivity (W/m·℃)	Linear Expansion Coefficient (10^{-6}/℃)
100	7.97	523	33.1	10.9
200	7.37	553	32.0	11.4
300	6.77	583	30.8	12.1
400	6.17	617	29.8	12.6
500	5.55	661	29.0	12.8
600	4.86	735	28.0	13.0
700	4.03	847	26.8	13.2

Other property data such as thermal creep, fatigue for the 350kg ingot is accumulating and the optimization of the melting technical for the larger ingots is underway. In addition, other manufacturing technologies for the construction of the TBM are being developed, such as hot isostatic pressing (HIP) and electron beam welding [15].

4.2 Function materials

Two kinds of the solid tritium breeder, Li_2TiO_3 and Li_4SiO_4, have been investigated in China. Preliminary test results show that Li_2TiO_3 pebbles prepared by using sol-gel method have good surface feature [16] and Li_4SiO_4 pebbles prepared by Freeze-sintering process have

good mechanical intensity (the average crush load is 50N). Lithium orthosilicate pebbles are one of the options of ceramic breeder TBM in China.

The Lithium orthosilicate pebbles have been fabricated with three steps: synthesis powder, sphericizing and sintering. Lithium orhtosilicate powders have been synthesized by using solid state reaction of a mechanical mixture of Li_2CO_3 and SiO_2 corresponding to Li/Si=4.0.[17]

Weight changes during heating the mixture were investigated by thermo-gravimetry (TG) with a heating rate10℃/min in the temperature range of RT-1000℃ under N_2 atmosphere. It can be seen from Fig.15 that the weight loss of about 40% occurred between 550℃ and 900℃, the significant weight lost took place at 700℃. This is because CO2 released during reaction. The overall weight of the sample remained constant until 950℃ as shown by TG curve.

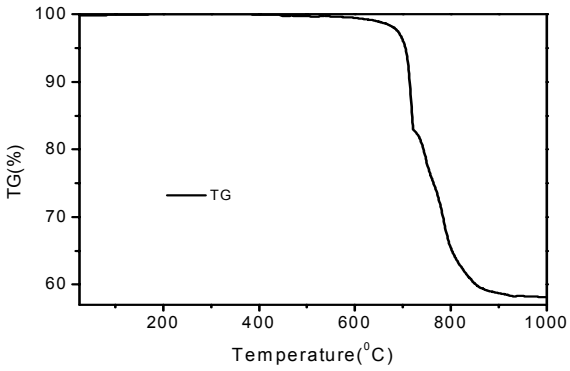

Fig. 15. TG curve of Li_4SiO_4 obtained by solid state reaction.

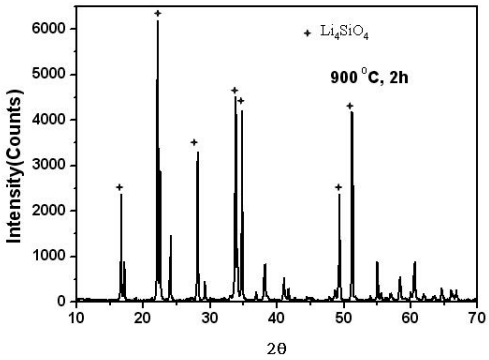

Fig. 16 XRD patterns of Li_4SiO_4 by solid state reaction method.

The phase composition was characterized at room temperature by X-ray powder diffraction (XRD). As seen in Fig.16, only diffraction peaks of Li_4SiO_4 were observed on the XRD patterns when the mixtures were calculated at 900℃ for 2h, indicating that Li_4SiO_4 phase could be obtained by the solid state reaction. Fig. 16 shows XRD patterns of Li_4SiO_4 by the solid state reaction method.

The extrusion-spheronisation-sintering process was selected for sphericity of Li_4SiO_4 pebbles, as it proved to be the most appropriate one to obtain the goal characteristics. In

addition, the process makes use of conventional techniques of the ceramic industry; therefore, industrial production is not expected to raise any significant problem. Presently, this step is under development.

Exploration study of Be pebbles fabrication technology has been performed. Related performance test is on going. Be alloy pebbles are prepared by powder metallurgical (PM) methods.

4.3 Helium experimental loop

In order to validate the technical feasibility of the TBM design, it is indispensable to test mock-ups of TBM components in a helium loop under realistic pressure and temperature profiles [18,19]. Therefore, SWIP plans to build a small-scale 8 MPa helium test loop with mass flow rate of 0.35 kg/s. The preliminary design of the helium test loop for HCSB TBM has been completed. The test loop diagram for circulator R&D is shown in Fig.17. The loop includes the primary helium loop and the secondary water loop. Main components of the primary loop include a cooler, circulator, control valves and pipe work. There is a pressure control unit for system evacuation, helium supply and protection against overpressure. Fig.18 shows the loop diagram for TBM components testing. Relevant equipment investigations, including compressor, cooler, and the other key studies are ongoing.

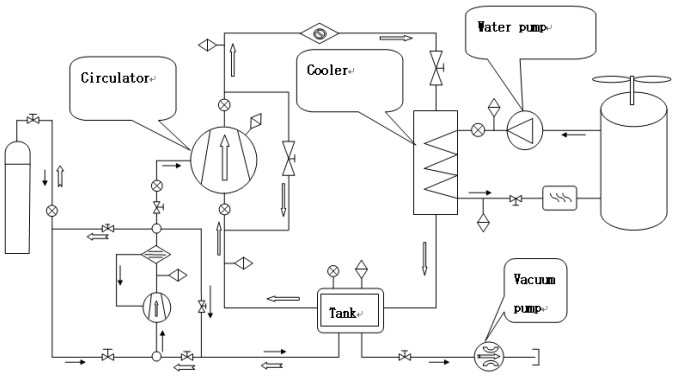

Fig.17. He test loop diagram for circulator

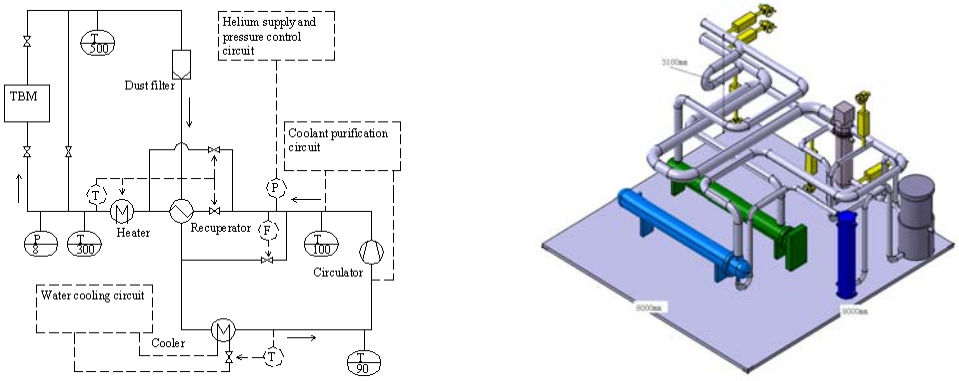

Fig.18. He test loop diagram for TBM components

5. Summary

The current progress on the modified design of the HCSB TBM and corresponding performance analyses were reported. Calculation and analyses results show that the modified HCSB TBM design is feasible and can be developed within the existing domestic

technologies. Further work on the HCSB TBM module and system design will be updated and the corresponding optimization of the structure design as well as ancillary subsystem parameters are selected based on the ITER operation condition and testing limitations. Related R&D on the structure material (CLF-1), function materials including Li_4SiO_4, Be pebble, and the development and construction of the helium test loop design are in progress.

Acknowledgement

This work was supported by a grant from the Major State Basic Research Development Program of China (973 Program，No. 2009GB108000) and the Key Program of the National Natural Science Foundation of China（No. 10835010）.

References

[1]. K.M. Feng, G.S. Zhang, X.Y. Wang, D.L. Luo, Z.W. Zhou, et al., Design Description Document for the Chinese Helium-cooled Solid Breeder TBMs (Draft Design Report), Oct. 30, 2007.

[2] K.M. Feng, C.H. Pan, G.S. Zhang, T. Yan, Z. CHE, et. al., Overview of design and R&D of solid breeder TBM in China, J. Fus. Eng. Des. 83 (2008) 1149-1156.

[3] ITER TBWG Members. Report from the re-established test blanket working group for the period of the ITER transitional arrangements (ITA) [R]. 2005.

[4] Hermsmeyer S, Gordeev S, Kleefeldt K, et al. Improved helium cooled pebble bed blanket [R]. FZKA 6399, 1999.

[5] ITER documents. Structural design criteria for ITER in-vessel components (SDC-IC), Appendix A: materials design limit data [R]. G 74 MA 8 R0.1, 2004.

[6] L.V.Boccaccini et al. Strategy for the blanket testing in ITER. Fusion Engineering and Design,2002,61-65:423-429.

[7] Load Specification (LS) – Annex of Project Integration Document (PID) ITER_D_222QGL v 3.0, July 2005.

[8] S.Suzuki et al. EM Analysis of Modules, Dynamic Analysis of the Key and Module 10 Design Improvement. ITER Design Task Report ITA 16-11,G 16 TD XXX FJ: I-1

[9] Pinghuai Wang, Jiming Chen, Shi Liu el al. Preliminary Results on the Research of CLF-1 Steel[R]. Presented at 9th China-Japan Symposium on material of advanced energy and fusion-fission engineering, Oct.23026,2007

[10] Zhi Chen，K.M. Feng, G.S. Zhang, T. Yan, C.H. Pan, Preliminary safety research for CH HCSB TBM based on FMEA method. Fusion Engineering and Design, 83:743–746, 2008.

[11] L.C. Cadwallader. Selected component failure rate values from fusion safety assessment tasks. INEEL/EXT-98-00892, INEEL, 1998.

[12] L.C. Cadwallader. Preliminary failure modes and effects analysis of the US DCLL test blanket module. INEEL/EXT-07-13115, INEEL, 2007.

[13] L. Zhang, Preliminary probabilistic safety analysis of CN HCSB TBM system, SWIP report, 2008.

[14] WANG Pinghuai, NOBUTA Yuji, HINO Tomoaki, Helium Retention and Desorption Behavior of Reduced Activation Ferritic/Martenstic Steel, Plasma Science and Technology, Vol.11, No.2, Apr. 2009

[15] Pinghuai Wang, Jiming Chen, et al. Progress of China RAFM Steel CLF-1 R&D, Ninth International Symposium on Fusion Nuclear Technology, Oct.11-16, 2009, Dalian, China.

[16] Xiaojun Chen, Xiaoling Gao, Deqiong Zhu and Heyi Wang, Fabrication development and preliminary characterization of lithium ceramic pebbles by wet process, 2nd Japan-China Workshop on Blanket and Tritium Technology (2008)107-111.

[17] Y. J. Feng, T.Y. Luo and K. M. Feng, Synthesis of Lithium Orthosilicate (Li_4SiO_4) powder, submitted to ISFNT-9 (2009).

[18] Ionescu Bujor, M, et al., Helium Loop Karlsruhe (HELOKA) – large experimental facility for the in-vessel ITER and DEMO components, 20th IAEA fusion energy conference, 2005

[19] G.Dell'Orco, et al., HE-FUS3 – European helium cooled blanket test facility for demo, Fusion Technology, 1996,1335-1338